Journal of Molecular Structure 1349 (2026) 143770

Contents lists available at ScienceDirect

Journal of Molecular Structure

journal homepage: www.elsevier.com/locate/molstr

Revealing the impact of the rotational isomerism onto photoluminescent properties of some ortho derivatives of benzophenone

Andrzej J. Kałka [a,b,*], Aleksandra Orlef [a], Agnieszka Kaczor [a], Andrzej M. Turek [a]

[a] Faculty of Chemistry, Jagiellonian University in Cracow, Gronostajowa 2, Cracow, 30-387, Poland
[b] Theory Department, National Institute of Chemistry, Hajdrihova 19, Ljubljana, 1000, Slovenia

ARTICLE INFO

Keywords:
Benzophenone
Rotational isomerism
Conformational analysis
Photoluminescence
Chemometric data modeling
TD-DFT simulations

ABSTRACT

Benzophenone (BP) scaffold, owing to its highly applicable photo-related properties, has been widespread among many branches of chemical research and industry. While the benzophenone molecule itself has been extensively studied towards the intrinsic mechanisms standing behind its prominent nature, yet its derivatives still tend to be under-explored in this particular regard. Coming across the disclosed imparity, throughout the present paper, a subject of rotational isomerism, anticipated to affect the BP frameworks substituted in the *ortho* position, is thoroughly investigated. In this respect, a bunch of *ortho* derivatives of BP are subjected to a systematic analysis carried out via both *in silico* DFT modeling and spectroscopic measurements (IR, UV–Vis). The obtained results show that the effect of rotamerism indeed applies to the studied group of compounds, as some of them reveal themselves in the form of multiple coexisting conformational isomers. What is more, as the indicated conformers are found to be characterized by substantially different emission profiles, the foregoing phenomenon is disclosed to have quite a remarkable impact onto the photoluminescence of the explored *o*-BP molecules.

1. Introduction

Benzophenone (BP), or more systematically diphenylmethanone (Ph_2CO), is a relatively simple organic compound, being highly recognizable for its pretty unusual behavior under the influence of UV light. In a nutshell, the latter trait involves an interplay of both singlet and triplet electronic states that enables the BP molecule upon excitation to lose the excess energy in several possible relaxation pathways [1–4]. While such distinctive photophysical properties have naturally captivated scientific interest and become the object of many research studies, as a matter of course, they have also started to be appraised in terms of practical applications. In the result, benzophenone, together with its various derivatives, can now be encountered as fairly common substrates in various branches of chemistry-related industry [4] including, among others, plastics and dyes production [5–7], cosmetics sector [8,9] or pharmacy [10,11].

Considering functionalization of the discussed diphenylmethanone compound [3], in general, it is achieved by attaching one (or more) substituents to the aromatic ring(s) of the core BP moiety in either *ortho* (2-), *meta* (3-) or *para* (4-) positions, out of which the last two (i.e. *meta* and *para*) tend to be most commonly selected [3,6,7,11]. However, from the fundamental research perspective, it is the *ortho* position, which appears to be the most compelling one. This is due to the fact that in such a case, the appended functional group remains in the immediate vicinity of the central carbonyl oxygen atom (see Figs. 1 and 2), with which it can effectively interact [12–15]. The latter on the other hand, may conceivably affect the properties of the entire molecule (not to be groundless, the example of *ortho*-hydroxybenzophenones, used as a popular sunscreen agents, can be adduced herein [8,9,16]).

As regards the structure of the above mentioned *ortho*-BP derivatives, according to the crystallographic data (cf. Fig. 1) [17,18], these most frequently occur in two dominant conformational forms, *syn* and *anti* (see Fig. 2) in which the pendant group X-Ph, takes properly the congruent and divergent positions with respect to the carbonyl oxygen atom, O=C (both of the latter being slightly skewed due to the sterical reasons). In brief, the former orientation (*syn*) is more frequently observed for the substituents comprising hydrogen atoms (and capable of forming hydrogen bonds with O=C), while the latter one (*anti*) is spotted for the pendants that are highly electronegative (electrostatic repulsion) [15,18,19]. Yet, it can be noted at this point that despite dozens of individual structures deposited in crystallographic databases (cf. Fig. 1), only a few papers published so far have actually tackled the

* Corresponding author at: Faculty of Chemistry, Jagiellonian University in Cracow, Gronostajowa 2, Cracow, 30-387, Poland.
E-mail address: andrzej.kalka@uj.edu.pl (A.J. Kałka).

https://doi.org/10.1016/j.molstruc.2025.143770
Received 26 May 2025; Received in revised form 20 August 2025; Accepted 24 August 2025
Available online 25 August 2025

issue of systematic conformational analysis within the group of *ortho*--benzophenones [18,19].

Nonetheless, the subject that remains even more uncharted as regards the foregoing systems of *o*-BPs is the "dynamic" aspect of the outlined conformational isomerism. To be specific, for the samples in the solid state, the orientation of both the aromatic rings is in general fixed, and hence remains uniform for all the individual molecules therein. However, when the corresponding crystal is liquified (or heated [20,21]) the aforesaid moieties become more flexible and gain the possibility to rotate around the C—C bond linking them to the carbonyl fragment. In the result, some molecules can change their conformations, forming isomeric entities known as the rotamers [19,22]. If the latter are persistent enough, a state of equilibrium is established between them and the sample eventually takes on a multicomponent character.

Although the aforesaid rotational isomers share the same topology, yet, due to the already mentioned interactions between the X-Ph pendant and the central oxygen atom O=C, they can show quite significant differences in both (photo)physical and (photo)chemical properties [14,21,23,24]. While such a feature should make the individual rotamers experimentally distinguishable, yet, their detection has been explicitly reported so far for only two *o*-BP compounds, comprising chloro- [25] and bromo- [20,21] substituents (which was achieved throughout the analysis of Raman and electronic spectra, respectively). Taking into account certain (in)direct indications on the conformational multitude expected for the akin systems that can be inferred from a number of papers [14,19,23,24,26–29], this tends to be a little unsatisfying, and thus naturally creates an opening for a further investigation on the outlined matter. Although the latter would be of rather fundamental character, yet, through the prism of the benzophenone scaffold universality [3], the resultant findings may be translated over time also into the more sensible dimension.

In reference to the last but one remark ending the preceding synopsis, the principal aim of the undertaken study (and so of this paper), is to take a deeper insight into the indicated phenomenon of rotational isomerism, and its implications, within the *ortho*-substituted benzophenone derivatives. For this purpose, both theoretical and experimental research methods will be complementarily harnessed, which shall facilitate the foregoing investigation as well as increase its cognitive value [30]. The inquiry is about to start with a preliminary quantum-chemical study launched for an ample set of *o*-BP molecules, covering different types of elementary organic substituents. Based on the resultant indications, the compounds for which the concurrent existence

Fig. 2. Schematic depiction of *syn-anti* rotational isomerism within the *ortho*-benzophenone frameworks.

of two (or more) conformational isomers is found to be plausible, are to be identified and submitted to further investigation. In this respect, for the selected *o*-BP species, the respective experimental UV–Vis and IR spectra would be measured and subjected to a thorough analysis. The latter, supported by chemometric methods devised for spectroscopic data modeling, should eventually disclose whether the phenomenon of rotamerism could be spectroscopically discerned in the studied molecular systems [31].

2. Methods and materials

2.1. Computational details

2.1.1. Computational methodology and resources

All the quantum-chemical calculations were performed on the HPC Ares (ACC Cyfronet, PLGrid) and Eagle (PSNC, PLGrid) clusters, adopting the Density Functional Theory (DFT) methodology implemented in the Gaussian 16 (rev. A.03) package [32]. In order to deal with molecules in their excited electronic states, Time Dependent (TD) extension to DFT, framed with the Tamm-Dancoff Approximation (TDA), was utilized. To carry out the computations, B3LYP (IR) and M06–2X (UV–Vis) functionals, additionally augmented with Grimme D3 dispersion correction, and a 6–311+G** basis set were harnessed, selection of which was drawn on the dedicated benchmark reports [33–35] as well as some preliminary computations. Inclusion of the solvent effects was achieved through the use of the implicit PCM solvent model.

2.1.2. Scheme of computations

The initial atomic coordinates, defining the investigated molecules, were based on the crystallographic framework of benzophenone (Cambridge Structural Database, CSD) [17], that was subsequently expanded

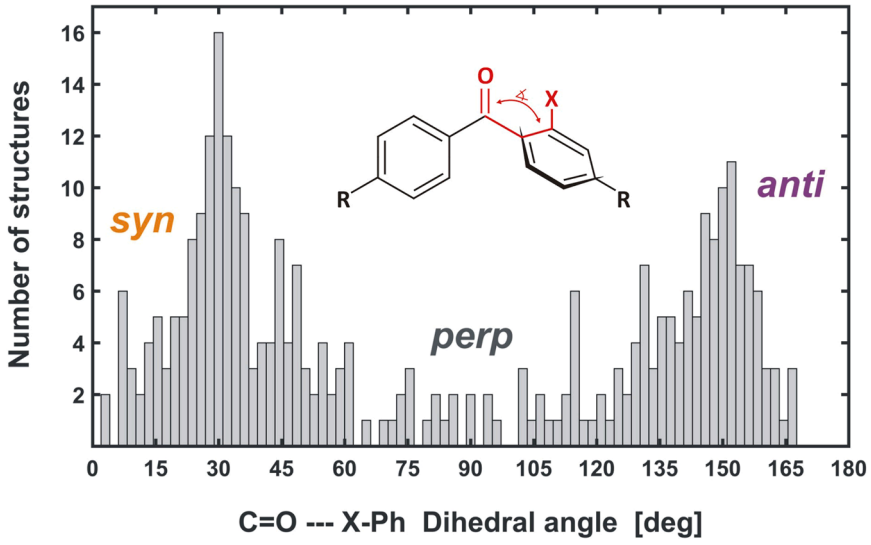

Fig. 1. Distribution of C=O — X-Ph dihedral angles within crystallographic structures deposed in CSD database [17], containing the *ortho*-benzophenone fragment. The majority of compounds take skewed *syn* or *anti* conformations, though for some of them the perpendicular one (*perp*) can also be observed.

with appropriate substituents. These were next subjected to optimization (no symmetry constraints) in the vacuum conditions and validated via vibrational analysis, the latter of which was for the selected species rerun also in the anharmonic approximation (GVPT2 model, simulation of the IR spectra) [36].

In order to evaluate energetic profiles related to revolving of the substituted arene ring with respect to the carbonyl fragment (*anti* ↔ *syn* isomerism), series of relaxed potential energy surface (PES) scans were performed. These were generated by fixing and gradually changing of the dihedral angle between the carbonyl oxygen atom and the outward atom in the ortho position of the phenyl moiety. The structures corresponding to the transition states (TS) found this way were next subjected to reoptimization, results of which were eventually validated by the vibronic analysis.

In the following step, the analogical procedure (but without the anharmonic calculations) was employed for the molecules in their first singlet (S_1) and triplet (T_1) excited states, for the purpose of which the afore-mentioned TDA approach was used (into the bargain, the cross-reference triplet-state UHF computations [37] were also launched). In the process, energies and oscillator strengths of corresponding vertical electronic transitions ($S_0 \leftrightarrow S_1$, $S_0 \leftrightarrow T_1$) were also naturally determined. Ultimately, for the chosen entities, by adopting the Franck-Condon methodology, vibrationally-resolved UV–Vis spectra were also simulated (in the case of phosphorescence, a unitary transition dipole was used) [38].

Finally, with an aim to roughly explore the impact of solvation onto the studied systems, the selected molecules were "submerged" into several continuous media characterized by different polarity and, after the reoptimization procedure, subjected to the vibronic analysis.

2.2. Experimental details

2.2.1. Materials

The experimentally investigated *ortho* and *para* derivatives of the benzophenone compounds (BP-H), covering fluoro- (BP-F), cyano- (BP-CN), methyl- (BP-CH_3) and methoxy (BP–OCH_3) substituents, were purchased commercially (Ambeed, Alfa Aesar, Sigma-Aldrich) as high purity samples (99 %, 98 %, 95 %+). All the solvents involved in the spectral measurements (HPLC grade), i.e. acetonitrile (ACN), tetrachloroethene (TCE, C_2Cl_4) and dichloromethane (DCM, CH_2Cl_2), were additionally distilled prior to use.

2.2.2. Vibrational FTIR spectra

The obtained benzophenones (c.a. 30 mg) were dissolved in small volumes (1.0 mL) of tetrachloroethene (TCE), reaching solutions of c.a. 0.1 M. Due to their limited solubility, in case of BP-*o*CN and BP-*p*CN species, a few droplets (0.05 mL) of dichloromethane (DCM) were furthermore added to the samples. Such prepared solutions were then put into demountable barium fluoride (BaF_2) cells, adjusted to 50 μm and 100 μm pathlengths, depending on the measured signal intensity (max. absorbance on the level of 1.0). The FTIR spectra were recorded at the room temperature using a BioTools ChiralIR-2X™ spectrophotometer, at a spectral resolution of 2cm^{-1} (512 coadded scans) in the effective range of 850 – 4000 cm^{-1} (with the lower value limited by the used optical system).

2.2.3. Electronic UV–Vis spectra

From all of the acquired samples of benzophenone derivatives a set of respective solutions in acetonitrile, yielding c.a. 0.01 M, was prepared (c.a 15 mg / 5 mL) [39]. For the resultant melds, absorption spectra were then recorded in the range of 270 to 450 nm, using a Hitachi U-2900 spectrophotometer (10 mm quartz cells). In the next step, the appropriate solutions were poured into a purpose-designed quartz vessel (fluorometer 10 mm cuvette combined with a round-bottomed flask) in which they were degassed through three freeze-pump-thaw cycles. Subsequently, for such prepared samples, excitation-emission photoluminescence maps (EEM) were then collected using a Hitachi F-7000 spectrofluorometer (EX/EM slits set to 5 or 10 nm). In the final step, the aforesaid cuvette was unsealed and the outcoming maps were recorded for the aerated melds. All the spectral measurements were carried out at 25 °C with the use of Julabo F12-ED constant temperature circulator.

2.3. Spectroscopic data processing

2.3.1. Elements of chemometric data modeling

In principle, processing of the spectra collected during the performed measurements was to a great extent based on chemometric methods applied for modeling of the experimental data. Although the latter have been thoroughly described in the literature, yet, for the sake of convenience, some basic information on the adopted techniques will be briefly described in below.

Thereby, starting from the first principles, each spectrum $\mathbf{y}$ recorded for a given sample should consist of a finite number of lines (reflecting quantized transitions occurring for the component molecules), that are effectively blurred to a form of non-discrete spectral bands [40,41]. Mathematically, $\mathbf{y}$ may be then seen as a set of the Dirac delta functions $\boldsymbol{\delta}$ convolved with a bell-shaped broadening function $\mathbf{b}$, which in the Fourier domain (F – Fourier transform), can be denoted as [40,42]:

$$F\mathbf{y} = F(\boldsymbol{\delta} * \mathbf{b}) = F\boldsymbol{\delta} \cdot F\mathbf{b} \tag{1}$$

Since broadening in most cases results in a decrease of spectrum $\mathbf{y}$ informativeness (the fine structure starts to fade due to overlapping of bands), it is worth to consider how it may be effectively reduced. Incidentally, a direct way to achieve this is offered by a deconvolution operation [40,42] which, pursuant to the convolution theorem Eq. (1), shall allow to literally reverse the detrimental impact of $\mathbf{b}$ onto $\mathbf{y}$, eventually restoring $\boldsymbol{\delta}$.

$$F\boldsymbol{\delta} = \frac{F\mathbf{y}}{F\mathbf{b}} \approx F\mathbf{y} \cdot \mathbf{f_S} \cdot \mathbf{f_A} \tag{2}$$

However, due to a significant numerical instability, in practice, such a procedure usually is not feasible and has to be algorithmically refined. One of possible ways for doing so, known as self-deconvolution approach [40,41], is to avoid singularities in Eq. (2) by swapping the division operation into multiplication of $F\,\mathbf{y}$ with a coupled spreading function $\mathbf{f_S}$ (input filter), being illustratively equal to an inverse of $F\,\mathbf{b}$ (i.e. an exponential curve). Subsequently, the resultant product should be fine-tuned with an apodization function $\mathbf{f_A}$ (output filter), adjusted to dampen the emerging numerical inaccuracies (as well as some portion of instrumental noise). As an effect, the spectral bands at the output get significantly narrowed, eventually revealing the fine structure of the spectrum (see Fig. S.1) [40–43].

On the other hand, overlapping of the spectral bands may also stem from the composite character of the investigated sample and hence multiple sources contributing to the recorded signal (optically active chemical species). In such a case, an attempt can be made to decompose the measured (series of) spectra $\mathbf{Y}$ into their individual components. Assuming that the latter can be defined by some principal profiles $\mathbf{s}$ and $\mathbf{c}$ characterizing each of the n sources (e.g. emission and absorption profiles, as in case of the excitation-emission maps, EEM), $\mathbf{Y}$ can be brought to a following sum of outer vector products,

$$\mathbf{Y} = \sum_n x_n \cdot \mathbf{s_n}\mathbf{c_n^T} + \mathbf{R} \tag{3}$$

where x are intensity scaling factors (amplitudes) and $\mathbf{R}$ stands for signal residuals (such as background, artifacts and noise) [44,45]. Then, if at least one set of either $\mathbf{s}$ or $\mathbf{c}$ vectors is clearly specified, the aforesaid task of spectra separation remains rather straightforward as it boils down to a series of rather basic matrix multiplication operations, referred to as Multivariate Curve Resolution (MCR) [44,45].

On the other hand, if both $\mathbf{s}$ or $\mathbf{c}$ are not well-defined prior to

investigation, factorization of the spectral data matrix **Y** can still be achieved using Singular Value Decomposition (SVD) algorithm [45,46],

$$\mathbf{Y} = \sum_{N} \sigma_N \mathbf{u_N} \mathbf{v_N^T} = \sum_{n} \sigma_n \mathbf{u_n} \mathbf{v_n^T} + \mathbf{R} \quad (4)$$

which provides an universal set of N vectors **u** and **v** describing the investigated dataset. Although the latter do not possess a direct physical sense analogical to profiles **s** and **c**, still, together with the coupled amplitudes (singular values) σ, they create a good foothold for processing of the collected spectra [45–47]. To wit, basing on the aforesaid entities, it is possible to evaluate the effective number n of sources (components) contributing to the recorded signal ($n \leq N$), subject of which is addressed by Principal Component Analysis (PCA) [47], an hence purge it from the unwanted variance (**R** in Eq. (3) and Eq. (4), see Fig. S.2) [45,46]. Moreover, by adopting principles of Self-Modeling Curve Resolution (SMCR) [48–51], vectors **u** can be also used to estimate actual spectral profiles **s** Eq. (3) characterizing individual (species) sources n. In brief, in order to do so, all the spectra $\mathbf{y_i}$ within series **Y** has to be properly normalized and projected onto the formerly determined principal vectors **u**.

$$\mathbf{y_i} = \alpha_i \mathbf{u}_\alpha + \beta_i \mathbf{u}_\beta + \ldots \quad (5)$$

The contributions α_i, β_i, … coming from the consecutive vectors $\mathbf{u_\alpha}$, $\mathbf{u_\beta}$, … are then juxtaposed against each other and searched for (regular) patterns, which in conjunction with some boundary conditions (e.g. nonnegativity of signal) [31,48–51], would allow to outline the sought individual profiles **s** (see **Fig. S.3**) and, thereby, eventually decompose the explored spectra **Y** Eq. (3).

2.3.2. Vibrational FTIR spectra

In the first step of the processing procedure the "crude" FTIR spectra recorded for the studied BP samples were background corrected by subtracting spectra measured for the corresponding solvents (TCE and TCE+DCM). Then, using *spline* curves fitting [52], each difference spectrum was manually refined (modeled) towards the removal of artifacts and the reduction of instrumental noise. In the next step, in order to enhance the visibility of their fine structure, the output spectra were submitted to a self-deconvolution procedure [40–42], based on the Fast Fourier Transform (FFT) algorithm (non-complex exponential and sigmoidal functions were used as input and output filters, respectively) [43]. Being corrected for the incurred artifacts, the resultant spectral profiles were eventually subjected to a peak analysis, that consisted in fitting a series of bell-shaped curves to the honed vibrational bands (for schematic depiction of the procedure, see Fig. S.1) [53].

2.3.3. Electronic UV–Vis spectra

As regards processing of the outcome of the UV–Vis measurements, pretreatment of both absorption spectra and the excitation-emission maps (EEM) began (and for the former also ended) with removal of the background signal done by the solvent subtraction operation (blank ACN sample). Subsequently, the EEM were corrected for the remaining artifacts originating from the scattering Rayleigh (and Raman) bands, which was achieved through a series of iterative SVD reproductions that allowed to sequentially eliminate the unwanted residual signals [45,46,54]. In the following step, the EEM preprocessed such way were factorized with SVD, explored with PCA and eventually reproduced with the indicated number of principal components [45–47]. With an aim of further refinement, the principal vectors used for the latter reproduction were additionally fine-tuned (smoothed) by FFT filtering [42,43,54]. Finally, basing on the related absorption spectra, the output maps were corrected for both primary and secondary inner-filter effects (for visualization of the procedure, see Fig. S.2) [55,56].

For the purpose of unmixing the investigated EEM, the component emission spectra were normalized to a unit area and subjected to the self-modeling procedure (SMCR) [48–51]. The resultant principal emission profiles, see Fig. S.3) were next used to decompose the corresponding EEM matrices (MCR approach), thereby unveiling the coupled excitation profiles [44,45]. Eventually, the individual spectra recovered this way, akin to their IR counterparts, after the self-deconvolution procedure, were submitted to the peak analysis.

2.3.4. Software and toolboxes

Processing of all the spectroscopic data collected during the research was performed in the MATLAB environment (v. 2015a) [57], supplemented with an occasional usage of the Origin Pro software (v. 9.1) [58]. All the MATLAB routines and scripts employed during the study were developed individually by the Authors [43,45] on the basis of native functions implemented therein.

3. Results and discussion

3.1. Conformational diversity of ortho-substituted benzophenones

Following the workflow scheme outlined in the introductory part, the present study began with a systematic series of conformational analysis, carried out for the benzophenone scaffold substituted in the *ortho* position with 14 different minor organic pendants (see Table 1). These were selected to cover the bulk of common organic functional groups, including alkanes, halogens, alcohols, ethers, carboxylic acids, esters, amines, nitriles and nitro compounds. The scrutiny itself effectively comprised scanning of relaxed potential energy surfaces (PES), depicting rotation of the pendant-containing aryl ring (X-Ph) with respect to the central carbonyl moiety (see Fig. 1). While graphical illustrations of such scans can be found in figures Figs. 3 and S.4, the characteristics of the calculated PES extrema, indicating the energetically stable structures as well as the transition ones, are summarized in Tables 1 and S.1. For comparison, wherever it was available, experimental structural information on the studied compounds acquired from the CSD database has also been provided therein.

By analyzing the obtained results, several important observations can be made. Firstly, not all the considered molecules are found to actually demonstrate the presumed multiplicity of rotameric isomers. To specify, in case of the BP scaffolds comprising carboxylic and nitro groups, only one structure (or in practice the ensemble of akin structures), resembling a perpendicular (*perp*) conformation, is indicated to be formally stable in terms of the PES criteria (see Fig. S.4). This may be related to the steric effects stemming from the size of the aforesaid pendants, that compels them to take a position providing the most decent amount of space. Nevertheless, for all the 10 leftover entities (out of initial 14), as many as two minima on PES, corresponding to *anti-* and *syn-like* conformations can be distinguished, which constitutes a prerequisite for the rotational isomerism to be applicable for the explored frameworks. However, taking into account the relative energies characterizing the individual rotamers (Table 1), the aforesaid phenomenon can be inferred not to be actually pertinent for both hydroxy- and amino- benzophenone, as well as for their charged derivatives. Namely, the divergence in the referred quantities (exceeding 20 kJ/mol, cf. Table 1) clearly indicates that, in practice, the foregoing compounds take only one privileged set of conformations, which enables to either form the intramolecular hydrogen bonds (*syn,* BP-OH, BP-NH_2, BP-NH_3^+) [19,23,26], or to separate the negatively charged oxygen atoms (*anti*, BP-O^-) [19]. On the other hand, for the remaining BP-F, BP-Cl, BP-CH_3, BP-CN, and BP–OCH_3 moieties, simultaneous occurrence of the two distinct rotational isomers ensembles appears to be quite plausible, as the estimated abundances of both *anti-* and *syn-like* species remain at the similar order of magnitude (greater that 10 %, see Table 1). Consequently, it is the above listed compounds that shall be in the first instance subjected to the more insightful investigations on the perceptible symptoms of the phenomenon of rotamerism.

Table 1
Output of the conformational analysis performed for the set of 14 considered *ortho*-derivatives of benzophenone. The first five columns provide structural information on the studied molecular systems (dihedral angle between the pendant, X-Ph, and the central carbonyl fragment, C=O), while the remaining three – their thermodynamic characteristics (free enthalpies, ΔG, of *anti* → *syn* transition, the related energetic barriers, ΔG#, and Boltzmann populations of the minor isomer, respectively). For the complementary results obtained with the M06–2X functional, see Table S.1.

-X	EXP (CSD)		CALC (B3LYP / 6–311+G**)					
	Dih [deg][a]	N	Dih [deg]			$\Delta G_{a\rightarrow s}$ [kJ/mol]	$\Delta G^{\#}_{a\rightarrow s}$ [kJ/mol]	Minor pop.
			anti	*syn*	TS			
H	28.8	6	29.8		90.0	-	13.0	-
CH_3	40.4	1	123.3	42.3	88.7	−1.9	4.3	32 %
Cl	115.0	2	123.1	63.3	73.1	3.1	8.8	22 %
CN	44.0	1	128.2	49.2	81.9	3.4	8.3	20 %
$COOCH_3$	58.6	1	119.7[b]	-[c]	-	-	-	-
	90.4	1						
COOH	104.0	4	115.1[b]	-[c]	-	-	-	-
	69.1	1						
COO^-	79.9	1	114.1[b]	-[c]	-	-	-	-
F	132.1	1	135.9	51.4	83.5	4.9	9.8	12 %
NH_2	17.2	4	140.1	19.2	97.2	−19.1	8.6	< 0.1 %
NH_3^+	-	0	133.7	17.6	94	−44.5	9.0	< 0.1 %
NO_2	-	0	125.4	-[c]	-	-	-	-
OCH_3	142.3	2	131.7	60.2	75.9	5.9	11.0	9 %
OH	7.4	5	144.1	12.7	93.5	−25.6	14.4	< 0.1 %
O^-	-	0	157.1	29.9	81.3	23.1	37.2	< 0.1 %

[a] Mean values of dihedral angles, averaged for N specified structures.
[b] The values of the dihedral angle effectively reflect the *perp* conformation (see Fig. 1).
[c] No formal minimum corresponding to the *syn* conformer was detected on PES (see Fig. S.4).

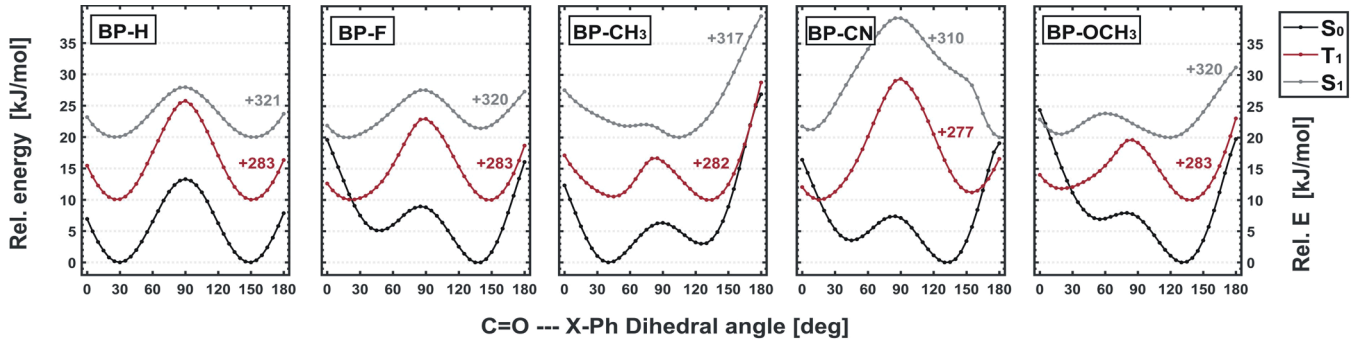

Fig. 3. Potential energy profiles determined (M06–2X) for the studied BP molecules in their ground (S_0) and excited states (S_1, T_1), related to revolving of the *ortho*-substituted phenyl moiety (X-Ph) with respect to the central carbonyl fragment (C=O). For clarity, all the depicted curves are vertically shifted to the common energetic scale (the applied shifting factors are marked with gray and red numbers, respectively).

3.2. Rotational isomerism at the molecular level

Pursuant to the conclusions drawn from the above-stated pre-screening procedure, the consecutive part of the present inquiry shall bend over the four subtypes of BP scaffolds, comprising halogen, alkyl, nitrile and ether functional groups, being represented accordingly by fluoro- (BP-F), methyl- (BP-CH_3), cyano- (BP-CN) and methoxy- (BP–OCH_3) benzophenone (as it is already described in literature [25], BP-Cl has been eventually decided not to be examined in the present research). Consequently, for all the above molecules (as well as the BP-H moiety as a reference), the rotation-related PES scans were launched once again, this time taking into consideration also the first excited singlet (S_1) and triplet (T_1) states, being most relevant as regards the forthcoming UV–Vis spectra analysis (Kasha rule [59,60]).

Looking at the resultant energetic profiles (Fig. 3), it can be noticed that for all the studied compounds, presence of as many as two stable ensembles of rotational isomers, referred henceforth simply as to *syn* and *anti* rotamers (or conformers), can be observed for each of the examined electronic states (this in a sense goes against the former reports on BP-Br, for which an additional *perp* conformation, most probably being an artifact, is predicted to be stable in the S_1 state [21]; for further commentary confer to Fig. S.5). Yet, the relative energies characterizing the foregoing conformers in their excited states are in general much more even as compared to those related to the ground state (Table 2), which theoretically should trigger the reequilibration process to take place upon the excitation. However, the latter may be effectively hampered by the energetic barriers separating both the isomers, being at the time noticeably increased in over half the cases (Table 2, Fig. 3; cf. NEER principle by Havinga [61,62]).

From the structural point of view, it can be additionally pointed out that the individual conformers in the S_1 and T_1 states alter in the degree to which the substituted phenyl ring is tilted towards the central carbonyl fragment (Fig. 1), becoming generally less internally skewed than their S_0 counterparts (Fig. 3). Such an effect, additionally combined with reshuffling of the electronic structure, results then in a drastic decrease in the dipole moments observed for the foregoing entities upon their excitation (Table 2) which, just to mention, may have quite a significant impact onto their electronic spectral properties (cf. Section 3.4) [38,63,64].

In the subject of the aforesaid dipole moments, being noticeably different for the individual rotamers (Table 2), it also seems reasonable to at least roughly evaluate a possible impact of solvation onto the investigated molecules. Namely, the solvent environments of different polarity may additionally favor one particular conformation

Table 2
Collation of calculated (M06–2X) geometric (dihedral angles, dipole moments, RMSD) and thermodynamic parameters (cf. Table 1) characterizing the five studied *ortho*-benzophenone molecules with respect to *anti-syn* isomerism. For the complementary results obtained with B3LYP see Table S.2.

State	Dih [deg]			μ [D]		RMSD [Å][a]		$\Delta G_{a\rightarrow s}$ [kJ/mol]	$\Delta G^{\#}_{a\rightarrow s}$ [kJ/mol]	$K_{a\leftrightarrow s}$	Min. pop.
	anti	syn	TS	anti	syn	anti	syn				
BP-H											
S_0	29.4		90.2	3.13		-		0.0	13.6	-	-
S_1	25.7		89.2	1.60		0.097		0.0	8.7	-	-
T_1	27.0		89.8	1.48		0.133		0.0	15.2	-	-
BP-F											
S_0	137.7	47.3	85.6	2.89	4.33	-	-	4.7	10.3	0.15	13 %
S_1	139.6	18.3	87.5	1.99	3.06	0.215	0.219	−1.5	7.5	1.8	64 %
T_1	147.8	22.1	87.6	1.53	2.83	0.114	0.069	−1.0	12.7	1.5	60 %
BP-CH_3											
S_0	125.8	40.5	88.8	3.29	2.70	-	-	−2.6	3.9	2.9	26 %
S_1	104.4	51.4	73.2	2.73	0.20	0.091	0.309	1.1	4.7	0.65	61 %
T_1	132.5	44.3	82.7	1.70	1.27	0.110	0.261	−6.6	6.9	14.2	7 %
BP-CN											
S_0	132.0	45.0	84.0	3.96	6.90	-	-	4.0	9.5	0.20	17 %
S_1	179.6	5.9	86.2	0.86	6.46	0.802	0.456	2.4	21.6	0.38	28 %
T_1	151.4	13.8	87.6	2.88	6.01	0.209	0.356	0.6	18.9	0.79	44 %
BP–OCH_3											
S_0	131.7	55.3	78.9	4.39	3.08	-	-	6.8	11.4	0.06	6 %
S_1	119.4	18.5	60.1	3.91	0.15	0.147	0.478	2.9	8.4	0.31	23 %
T_1	137.7	19.3	82.9	3.16	1.38	0.125	0.449	2.5	11.6	0.36	27 %

[a] The root mean square deviations (RMSD) determined with respect to the S_0 structures.

(possessing, respectively, lower or higher dipole moment), thereby affecting the thermodynamic equilibria between the *syn* and *anti* isomers [65]. And so, as it turns out, such an effect indeed takes place in the explored systems, which is clearly indicated by the computations comprising embedding of the studied benzophenone entities into various polar media (Fig. 4, Table S.3). Moreover, the outlined shifting of the equilibria appears to be pretty substantial, eventually leading to a remarkable increase in the relative populations of the minor rotamers [65], which remains propitious in reference to the forthcoming experimental part of the research.

3.3. Vibrational IR spectra

To make a brief recapitulation, thus far all the foregoing quantum-chemical predictions seem to support the surmise that the considered BP-F, BP-CH_3, BP-CN and BP–OCH_3 molecules undergo the rotational isomerism phenomenon. Thereby, the aforementioned compounds may

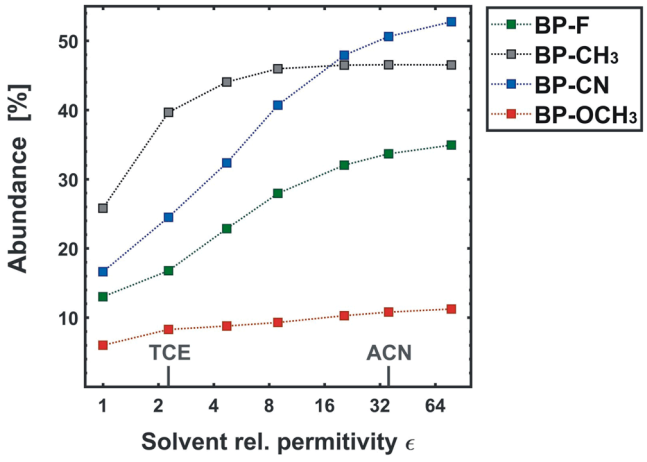

Fig. 4. Influence of solvation onto the thermodynamic equilibria between *anti* and *syn* rotamers (M06–2X), shown on the abundances of minor isomers evolving with the increasing polarity of the solvent environment (expressed by dielectric constant, ε). Solvents used in the experimental part of the study (i.e. tetrachloroethene and acetonitrile) are indicated with TCE and ACN markings, respectively. For the complementary B3LYPresults, see also Table S.3.

be expected to exist in the form of two stable isomers, *syn* and *anti*, both occurring in tangible abundance. However, it remains uncertain if the latter species can actually be detected in the experiments, that is, whether they are spectroscopically distinguishable.

Having taken a cue from the reports on akin cases [25,65,66], in the first attempt to address the above issue, the Authors decided to resort to vibrational spectroscopy techniques. Consequently, at the onset, for all the considered benzophenone scaffolds the infrared (IR) absorption spectra were simulated according to the anharmonic approximation [36]. The resulting spectral profiles, corresponding to *syn* and *anti* conformers, were then cross-referenced against each other, in pursuit of identifying some characteristic marker bands that would allow for identification of the abovesaid individuals. The performed analysis unveiled the presence of several such marker signals (Fig. 5). These include in particular the band due to the fundamental C=O stretching vibration ($\nu_{C=O}$, ~1700 cm^{-1}), showing different wavenumbers for the aforesaid conformers, and in the second place, case-specific bands related to the ν_{CC} stretching, (~1600 cm^{-1}), δ_{CCH} bending (~1450 cm^{-1}) and mixed $\nu_{CC}+\delta_{CCH}$ (1300–1100 cm^{-1}) vibrations [67]. Against this background, it may be then conjectured that it should be possible to discern the foregoing *syn* and *anti* isomers from the experimentally recorded IR signals.

Pursuant to the above premise, for all the investigated *ortho*-benzophenone compounds, as well as for their *para* counterparts, infrared absorption spectra were measured, using tetrachloroethene (TCE) as a solvent (the latter was found to ensure both high solubility and matching spectral window). The acquired spectra were then subjected to the digital enhancement procedure (self-deconvolution [40,42] combined with curve fitting [53], see Fig. S.1), targeted at unveiling the very structure of the initially entangled bands. Subsequently, the output signals were thoroughly analyzed and, in accordance with the theoretical predictions, one-by-one assigned to come predominantly from either *syn, anti* or both conformational forms (due to the natural limitations of the adopted approach, the latter assignment shall be then treated as inherently biased with some level of ambiguity).

Bending over the resultant spectral profiles shown in Figs. 6 and S.6, certain subtleties can be spotted, implying the composite character of the IR signals measured for the explored derivatives of benzophenone. And so, on the onset, it can be pointed out that spectra of the *ortho*-BP (Fig. 6), as compared to their reference *para* counterparts (Fig. S.6), possess an apparently increased amount of mutually overlapping component bands, which is particularly visible upon application of the

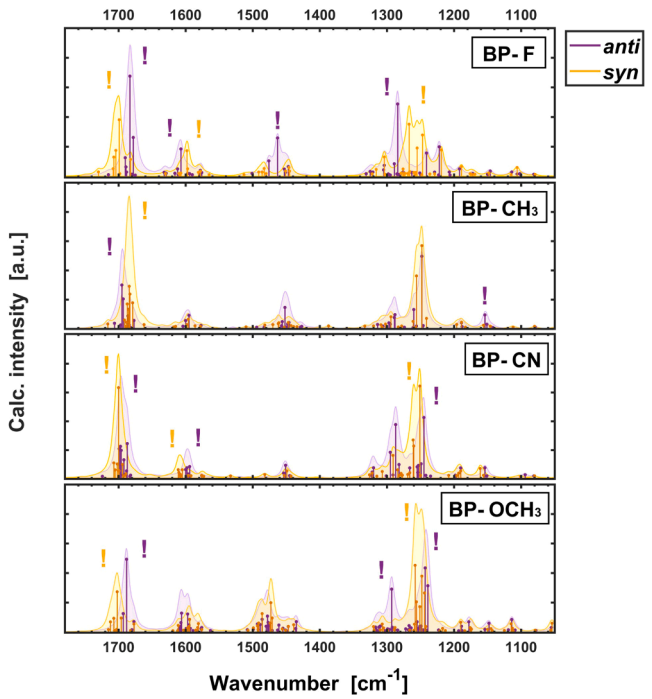

Fig. 5. IR spectra simulated for the four investigated *ortho*-derivatives of benzophenone (for the spectra of *para* counterparts, see Fig. S.6). With the exclamation points (!) the marker bands, assumed to enable identification of *syn* (yellow) and *anti* (violet) isomers, are indicated.

adopted resolution enhancement procedure. Taking into the account the same number of fundamental vibrational modes predicted by the first principles for both *o*-BP and *p*-BP entities, the outlined feature clearly suggests a non-unary nature of the samples corresponding to the former species.

In the above respect, the most prominent instance covers twinning of the $\nu_{C=O}$ stretching band, which consists in pairing of the main signal (1670 cm^{-1}) with a smaller peak, upshifted by c.a. 30cm^{-1} (1700 cm^{-1}). Since this pattern is not observed for the *para* isomers (Fig. S.6; to be precise, the secondary band appears also in the spectrum of *p*-BP-CN, but it remains of much lower intensity), it may be quite reasonably attributed to an occurrence of two distinct conformers, that differ in the spatial arrangement of pendants affecting the oscillating carbonyl group (cf. Fig. 5) [66]. Considering the less explicit examples, in the spectra of BP-F, BP-CH_3, BP-CN, and to a lesser extent also BP–OCH_3, conjectured to reflect mostly the IR signal of the dominant conformers, a few less evident odd-one-out inclusions can be identified (for details see Fig. 6), indicating a concurrent presence of the minor rotamer. These are particularly manifested in the spectral range related to vibrations of the hydrocarbon backbone, including ν_{CC} (1600–1615 cm^{-1}), δ_{CCH} (1500–1440 cm^{-1}) and mixed $\nu_{CC}+\delta_{CCH}$ (1220–1230 cm^{-1}) modes [67], which noticeably lines up with the prior theoretical predictions (Fig. 5).

While the adduced peculiarities observed in the spectra of *ortho*-benzophenones shall provide a firm argument to confirm the investigated systems as undergoing rotational isomerism, still, it can be desirable to estimate the quantitative implications of the latter phenomenon, that is to gauge the populations of the individual rotamers (X_a, X_s). In the very first approximation, this can be attempted by comparing integrated IR signals (A_a, A_s) coming solely from the *anti* and *syn* conformers, assuming that the matching bands remain of comparable intensity (Beer's law) [65,66]. In a more advanced approach, the former simplification should be repealed, taking into account differences in the fundamental intensities (I_a^0, I_s^0) of the collated bands (which incidentally can be derived from the performed quantum-chemical simulations).

$$\frac{A_s}{A_a} = \frac{X_s}{X_a}\frac{I_s^0}{I_a^0} \approx \frac{X_s}{X_a} = K_{a\leftrightarrow s} \tag{6}$$

Following the above scheme, for each of the analyzed *ortho*-BP compounds, suitable marker bands, assigned respectively to *syn* and *anti* rotamers, were selected (see numerical marks in Fig. 6) and compared with respect to the integral intensities. Subsequently, the resultant A_s/A_a ratios were scaled (6) by the DFT computed I_s^0/I_a° corrector factors (Fig. 5), eventually providing the coarse values of the equilibrium constants ($K_{a\leftrightarrow s}$) which, however, are found to vary considerably depending on the juxtaposed signals (Table 3). Still, even with the indicated bias

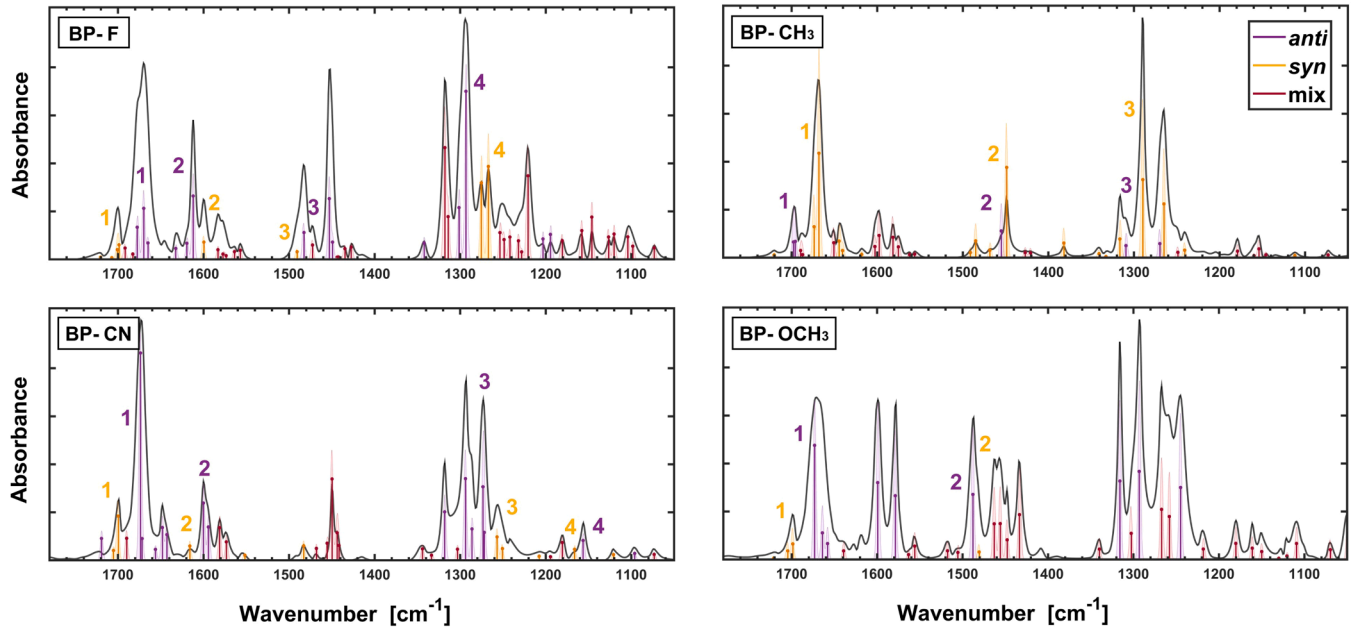

Fig. 6. Infrared spectra recorded for the investigated *ortho*-BP molecules (black line), decomposed into signals coming predominantly from *anti* (violet), *syn* (yellow) or both the conformers (red). The numbers 1–4 indicate the bands that were selected to estimate the relative abundances of the above species (Table 3). As regards the spectra measured for the *para* isomers, confer to Fig. S.6.

(being rather justifiable for the adopted rough estimation), the averaged values of the latter quantities appear to be in a rather high agreement with the theoretical predictions (Tables 2, S.3), which suggests that the hitherto outlined description of the explored *o*-BP systems is fairly accurate. Consequently, it can be concluded that the investigated *ortho*-benzophenone frameworks indeed occur in two conformational forms, out of which one is significantly more favored than the other. Yet, despite being remarkably less abundant (10–30 %), the minor conformer still has a tangible impact on the recorded infrared spectra and thus should not be neglected in meaningful spectroscopic considerations involving the discussed molecules.

3.4. Electronic UV–Vis spectra

Being intrigued by the thus far presented findings stemming from the infrared measurements, the Authors have eventually opted to explore the benzophenone compounds under question with respect to their electronic absorption and emission spectra. Following the well-proven workflow scheme, the corresponding inquiry was initiated with a series of quantum-chemical computations, aimed at outlining the nature of electronic transitions occurring within the studied BP frameworks. Remarkably, the outcome of such simulations turns out to provide particularly relevant insights on the foregoing species.

To begin with, for the considered molecules, absorption of light from the visible and near ultraviolet range shall incorporate only one $S_0 \rightarrow S_n$ transition, comprising solely the first singlet excited state S_1 (see Tables 3 and S.4, the subsequent $S_0 \rightarrow S_2$ excitation involves much shorter wavelengths, $\lambda < 250$ nm) [2,4]. The energy of such excitation is predicted to be much the same for *syn* and *anti* conformers, which should be reflected in quite similar absorption spectra observed for both these entities (the latter may however differ in the fine structure, see Fig. S.7).

Table 3
Quantitative assessment of equilibria between *syn* and *anti* rotamers, estimated for the investigated *ortho*-BP systems on the basis of the measured infrared spectra (Fig. 6). The left-hand side of the table provides the characteristics of the collated IR bands (positions, ν_{max}, ratios of integrated absorbances, A_s/A_a, and predicted fundamental intensities, I_s^0/I_a^0, Fig. 5), while the two columns on the right side outline the derived Eq. (6) values of equilibrium constants ($K_{a\leftrightarrow s}$) and gauged abundances of the minor conformers.

Index	ν_{max} [cm^{-1}]		A_s/A_a	I_s^0/I_a^0	$K_{a\leftrightarrow s}$	Min. pop.
	anti	syn				
BP-F						
1	1677, 1669	1703, 1699	0.082	0.62	0.133	12 %
2	1612	1599	0.429	0.94	0.459	31 %
3	1483	1490	0.222	0.67	0.324	24 %
4	1298, 1292	1276	0.108	0.61	0.176	15 %
		1267	0.185	0.33	0.556	36 %
$K_{calc.}$ 0.14 (0.22)[a]		*Mean:* 0.24±0.14		0.38±0.17		24±10 %
BP-CH$_3$						
1	1699, 1696	1673, 1668	6.35	1.69	3.768	21 %
2	1456	1449	1.82	3.06	0.595	63 %
3	1316	1310	1.02	0.55	1.863	35 %
	1270	1290	4.72	1.52	3.101	24 %
		1265	3.87	1.28	3.034	25 %
$K_{calc.}$ 2.1 (1.2) [a]		*Mean:* 3.6 ± 2.2		2.5 ± 1.3		34±17 %
BP-CN						
1	1676, 1671	1702, 1699	0.125	1.22	0.102	9 %
2	1600, 1595	1616	0.088	0.79	0.110	10 %
3	1272, 1275	1253, 1257	0.353	1.36	0.260	21 %
	1287, 1294		0.286	1.54	0.186	16 %
4	1156	1166	0.253	1.04	0.244	20 %
$K_{calc.}$ 0.26 (0.52) [a]		*Mean:* 0.22±0.11		0.18±0.07		15±5 %
BP–OCH$_3$						
1	1678, 1672, 1665	1702, 1698	0.072	0.71	0.101	9 %
2	1488	1482	0.077	1.26	0.061	6 %
$K_{calc.}$ 0.09 (0.07) [a]		*Mean:* 0.08±0.01		0.08±0.03		8 ± 2 %

[a] Values predicted by B3LYP (**Table S.3**) for the *o*-BP molecules embedded in vacuum and TCE (brackets).

Nevertheless, the aforesaid similarity does not by far apply to the reverse transition, being $S_1 \rightarrow S_0$ fluorescence, energies of which noticeably diverge for the afore mentioned *syn* and *anti* individuals (the latter translate into spectral shifts ranging from 10 up to even 50 nm; cf. Table 3). The like divergence, though of slightly smaller magnitude, is also observed for the $T_1 \rightarrow S_0$ phosphorescence, assumed to be the main emission process manifested by the considered benzophenone scaffolds (ironically, being characterized with a relatively low quantum yield, rarely exceeding 0.01) [1–3,20,21,39]. Consequently, pursuant to the above indications it should be possible, through an insightful analysis, to tease out the traces of two separate components, contributing to the photoluminescence spectra of the examined *o*-BP compounds.

In accordance to the above premise, for all the studied *ortho* (and *para*) derivatives of benzophenone, the indicated spectra were measured in the form of excitation-emission maps (EEM). As a solvent, degassed acetonitrile (ACN) was used (selection based on aproticity [3,23,68], solubility and transmittance criteria). The emission profiles obtained this way, formerly subjected to proper pretreatment procedure (Fig. S.2), were then normalized and eventually collated against each other in Fig. 7.

Before advancing to the actual analysis of the acquired spectra, a particularly interesting finding made during the performed experiments should be highlighted herein. Namely, for virtually all the examined BP samples, the observed spontaneous light emission was, as expected, almost entirely suppressed upon their aeration (the oxygen contained in the air interacts with BP molecules in the excited triplet state, quenching the phosphorescent emission of light) [1,39]. However, for the *ortho*-BP-CN compound, such regularity does not occur at all. To specify, the signal measured for the aerated sample was found to remain practically unchanged compared to its degassed counterpart. This in turn indicates that the emission of the above mentioned species originates from a short-living excited state(s), being effectively unsusceptible to the presence of oxygen [69]. In the same vein, it is also worth mentioning in this place that the signal recorded for *o*-BP-CH$_3$ was found to be approximately two orders of magnitude lower than that for the other *ortho*-BPframeworks [16]. This, on the other hand, may testify in favor of the nonradiative relaxation mechanism, comprising excited-state intramolecular proton transfer (ESIPT), assumed to be prevailing for this molecule (the matter of which will be addressed in the following paragraphs) [14,70].

Taking on the interpretation of the measured spectra themselves, it can be commenced with the most trivial case of *para* isomers. Evidently, for all such compounds a relatively intense phosphorescence can be recorded [13], the very profile of which remains independent of the excitation wavelength (Fig. 7). In particular, this lines up perfectly well with the assumed unary nature of the corresponding samples, comprising only one kind of luminescent chemical species [59,60] (these, to be accurate, are surmised to exhibit also residual fluorescence [1,39]). Subsequently, the specific symmetry observed between the absorption and emission spectra (the former being less structured) suggests that the aforesaid molecules in their excited state possess a similar, but slightly more planar structure as compared to the ground state (criteria by Berlman) [63,64]. In this respect, remarkable compliance with the theoretical predictions should be additionally noted (cf. Fig. 3 and Section 3.2), which translates in particular into the high accuracy of the simulated spectral profiles (compare Fig. 7 with Table 4 and Fig. S.7).

Moving onto the *ortho* isomers, represented in the first instance by BP framework substituted with fluorine, the luminescence of the corresponding sample(s) cannot be viewed anymore as uniform, demonstrating variability related to the applied excitation line (see Fig. 7). Admittedly, in the aforesaid case of *o*-BP-F, such evolution is still pretty elusive and manifests itself in rather subtle changes noticed for consecutive vibronic bands. Nevertheless, with a use of the chemometric methods for signal analysis (PCA and SMCR, see Fig. S.3), it can be attributed to the presence of two separate components contributing to

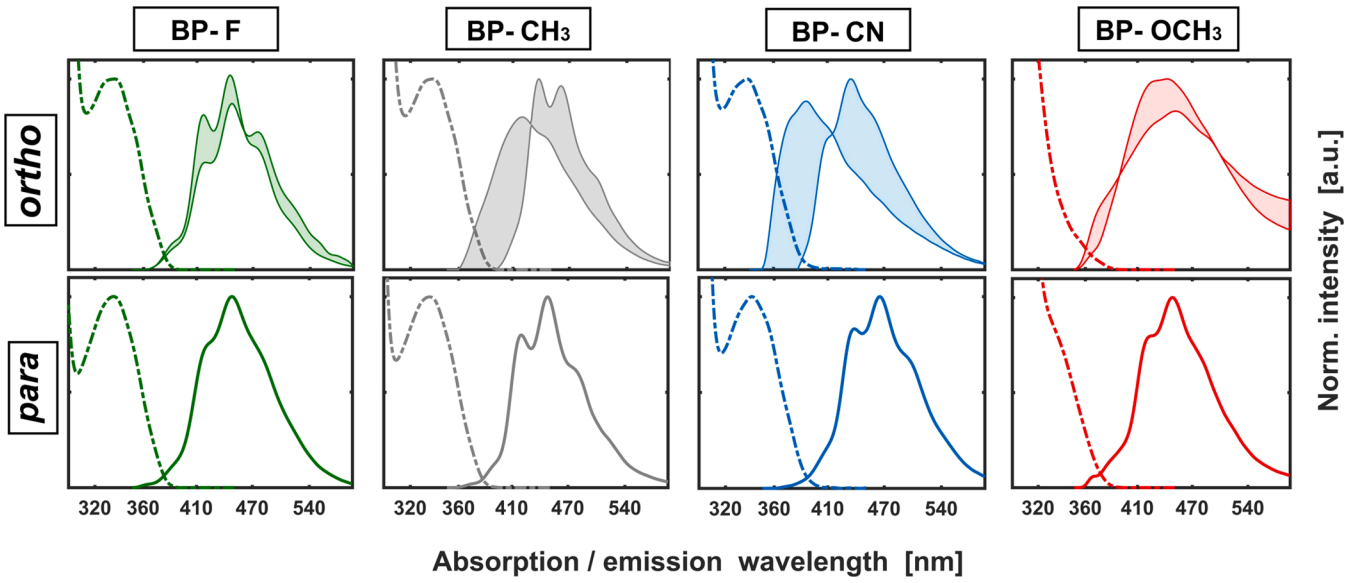

Fig. 7. Absorption (dashed lines) and emission (solid lines) spectra recorded for the explored *ortho* (upper row) and *para* (lower row) derivatives of benzophenone. With the spectral ribbons, dependence of the photoluminescence profiles on the excitation line is outlined. See also Fig. S.7 for the counterpart spectral profiles simulated theoretically.

Table 4
Wavelengths (in nm) corresponding to the selected vertical electronic transitions, determined for the five explored benzophenone scaffolds with TDA-M06–2X. For the predictions obtained with TDA-B3LYP, see Table S.4.

Transition:	$S_0 \rightarrow S_1$	$S_0 \rightarrow S_2$	$S_0 \rightarrow T_1$	$S_1 \rightarrow S_0$	$T_1 \rightarrow S_0$
BP-H					
Isomer	328.2	236.0	375.4	381.5	456.1
BP-F					
o-anti	325.7	239.2	371.8	382.6	461.2
o-syn	329.0	237.1	375.9	401.0	476.7
para	325.0	234.8	371.7	378.9	452.5
BP-CH_3					
o-anti	330.9	237.8	378.4	414.3	465.9
o-syn	330.7	242.6	377.4	393.1	454.9
para	327.0	237.2	374.0	380.9	455.0
BP-CN					
o-anti	328.9	243.1	377.1	484.7	483.9
o-syn	332.3	239.8	380.4	428.3	496.3
para	333.5	241.2	382.9	406.0	473.7
BP–OCH_3					
o-anti	326.3	256.0	372.7	397.1	459.8
o-syn	329.2	256.3	375.0	411.1	487.7
para	323.7	242.3	370.9	393.0	458.0

the recorded phosphorescence spectra. These, on the other hand, can be quite reasonably identified with two stable rotameric isomers inferred thus far for the discussed molecular system.

As regards ascribing the unmixed spectral profiles to the particular rotamers, shown in Fig. 8, in the considered case it can be quite reliably done pursuant to the indications provided by the DFT simulations (Fig. S.7), which fairly accurately reflect the aforesaid differences in the spectral fine structures characterizing the foregoing *anti* and *syn* species (threefold crown-like pattern vs the twofold slope-like one, respectively). By adopting such an assignment, it can be then derived that the former entity, dominant in the ground state, contributes to approx. 40 % of the overall signal intensity. Hence, assuming comparable emission yields of both the conformers [31] the analyzed system can be conjectured to undergo reequilibration upon excitation (see Tables 2 and S.3), which tends to be justifiable taking into account the long-lasting triplet states involved in the aforesaid process [1–3].

Having elucidated the variability of the electronic spectra measured for *ortho*-fluorobenzophenone, the more obscure issue of *o*-BP-CH_3, *o*-BP-CN and *o*-BP–OCH_3 compounds should eventually be addressed. In stark contrast to *o*-BP-F, the component signals contributing to the excitation-emission maps recorded for the foregoing species are reckoned to be distinctly different, exhibiting substantial spectroscopic shifts that reach even 50 nm (Fig. 8). Albeit such divergence has already been reported for similar multi-conformational systems [27,28,65,71,72], yet, before attributing its very origins to rotational isomerism, the Authors consider it appropriate to ponder also over two alternative explanations.

The first of the two (being rather tenuous) involves formation of the excimers in the corresponding samples, which results in occurrence of an additional band visible in the discussed spectra [20,73,74]. Yet, this interpretation is doubtful for (at least) three following reasons: (I) analogous behavior should also be observed for the other investigated BP-compounds (but it does not); (II) both the component signals tend to be fine-structured (which shall not be the case for the excimer emission bands [75]); and (III) appearance of the excimer emission band should not vary with the applied excitation wavelength [75] (but it does). Consequently, it can be pretty reasonably rejected.

The second (more reasonable) elucidation includes a dual mechanism of photoluminescence that comprises both phosphorescence and (delayed) fluorescence, occurring in comparable yields [1,39,60]. In such case, the appearance of two fundamental bands, shifted with respect to each other, seems quite evident (see Table 4). However, this hypothesis can as well be undermined by one substantial deficiency. Namely, in accordance with the Kasha rule, relative intensity of the afore mentioned bands should remain constant for all the excitation lines (excitation involves only one S_1 singlet state) [59,60], which is not met in the considered cases (Fig. 7).

Based on the above premises, it seems reasonable, by rejecting the less probable explanations, to conclusively attribute the two-component nature of the discussed spectroscopic signal to the phenomenon of rotamerism and thus to the coexistence of two equilibrated *syn* and *anti* rotamers. Still, the substantially high divergence of individual emission profiles characterizing the indicated entities may be considered suspicious. Yet, it turns out to actually line up quite well with reports on the alike benzil framework [28,65,71] and, even more importantly, with the theoretical predictions regarding the explored *ortho*-BP systems (Table 4), which shall be enlarged below.

Starting with the least intricate case, being the *o*-BP–OCH_3 molecule,

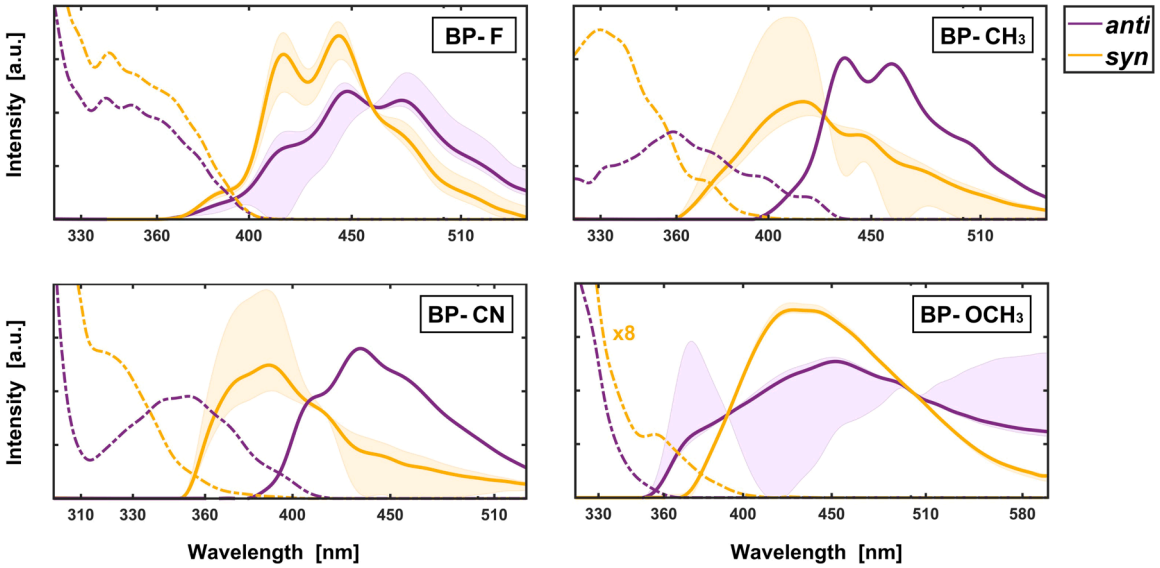

Fig. 8. Unmixed emission (solid lines) and excitation (dashed lines) spectra characterizing the four investigated *ortho*-benozphenone molecules. The spectral ribbons indicate the bias that naturally affects the photoluminescence profiles recovered with the self-modeling procedure (cf. Fig. S.3). For the spectra additionally enhanced with respect to their fine structure, see Fig. S.8.

assignment of the resolved spectral profiles to corresponding *syn* and *anti* conformers (Fig. 8) can be based on two indicators. First of them comprises relative contributions to the overall measured signal, equal to approx. 80 % vs 20 %, which strongly suggests the former component (marked in violet in Fig. 8) to be related to the dominant *anti* form (cf. Tables 2 and S.3). The second, on the other hand, concerns the very outline of the uncovered emission profiles. To wit, by collating the unmixed spectra, one of them (attributed to the *syn* rotamer) looks like being red shifted with respect to the other, at the same time having more diffused structure (see also Fig. S.8). Remarkably, the same feature is reflected in the spectra simulated for the foregoing species via DFT (Table 4 and Fig. S.7), which testifies to validity of the proposed elucidation.

Stepping to interpretation of the spectra acquired for the *o*-BP-CN compound, the first thing that catches the eye is a massive shift (over 50 nm) separating both the extracted emission profiles, which equally contribute to the recorded EEM (50 % vs 50 %, cf. Fig. 4). Apparently, this tends to stand in contradiction with the theoretical indications, according to which phosphorescence coming from the *anti* and *syn* rotamers should be observed in the comparable range of wavelengths (Table 4). However, at this point, the already indicated peculiar feature noted for the discussed *o*-BP-CN entity sample should be evoked. Namely, the spectroscopic signal recorded for its degassed and aerated samples (oxygen quenching) was reckoned to remain practically the same, pursuant to which it can be postulated to stem actually not from the spin-forbidden phosphorescence, but rather from the complementary fluorescence phenomenon [1,39]. Accordingly, it is the S_1 singlet electronic state that should be taken into the account while considering the indications by DFT, but not the formerly recalled long-lived triplet (T_1).

Coincidently, following such reasoning, the experimental results become perfectly consistent with their *in silico* counterparts. To specify, the considered drifting of the separated spectral profiles (Fig. 8) proves to be well correlated with the fluorescent emission wavelengths predicted respectively for the $S_1 \rightarrow S_0$ transitions related to *syn* and *anti* rotamers (Table 4; a red shift of >50 nm is anticipated for the *syn* form), which thereby allows for the unambiguous identification of the latter species. In addition, the component signal assigned to the *anti* conformer can be recognized as overlapping with the phosphorescence spectrum recorded for the *para* isomer (Fig. 7) which, being compliant with the quoted theoretical indications (Table 4), paves the way for the proposed elucidation to be conceded as trustworthy.

Having waded through all its forerunners, at the very end, the last and the most challenging case of the *o*-BP-CH_3 compound can be eventually discussed. Accordingly, the analysis may begin with an observation that the related photoluminescence spectra resemble a bit those recorded for the preceding *o*-BP-CN molecule. Namely, the unveiled principal emission profiles are visibly spread apart with respect to each other (by at least 20–30 nm, see Fig. 8), which (again) appears to go against the theoretical predictions (Table 4). Also, by analogy, one of the profiles being shifted towards the red appears to sort of overlap with the phosphorescence spectrum recorded for the *para* isomer (the latter being blue shifted by approx. 10 nm, see Fig. 7). Ultimately, both the components are once more found to almost equally contribute to the measured signal (55 % vs 45 %, cf. Table 4). Given all the above, the assignment of the unmixed spectra to the specific isomeric species can be inferred as a rather nontrivial task, the subject of which shall be thoroughly addressed herein.

Accordingly, as a starting point, the indicated red-shift of one of the component profiles relative to the *para* isomer spectrum can be taken (Fig. 7). This is because such a feature is quite well reflected by the supplementary DFT simulation, pinpointing it to the $T_1 \rightarrow S_0$ transition occurring for the *anti* rotamer (Table 4). By adopting this premise, the remaining, blue-shifted profile has to be then naturally attributed to the *syn* conformer. While the latter does not quite match the theoretical phosphorescence characteristics of the aforesaid entity, yet, it tends to line up quite well with the predictions regarding the complementary $S_1 \rightarrow S_0$ transition (Table 4). Consequently, it appears reasonable to ponder whether the emission of the foregoing *syn* rotamer can be associated rather with fluorescence than phosphorescence.

Remarkably, such a surmise turns out to sound sensibly taking into account the ultrafast proton transfer (ESIPT) expected to occur for the considered species [14,70]. To specify, the quoted phenomenon offers an alternative nonradiative relaxation pathway, competing with both the aforesaid photoluminescent ones. However, by comparing the time scale of all the above processes, it is phosphorescence, which is more prone to be overwhelmed by ESIPT [6,14]. Consequently, it causes fluorescence to become the dominant mechanism of emission (as regards the coupled photoenol, its emission is reported to be shifted far to the red as compared to the *keto* form [14] and thus should not be included in the present considerations).

To round up, although the above presented explanation (Fig. 8) can

be regarded as a conjecture rather than a formal proof, yet, it is believed to provide the most reasonable interpretation of the spectra recorded for the *o*-BP-CH_3 compound, which thereby concludes the list of the explored *ortho*-benzophenone frameworks (on the margin, an alternative assignment of the pure spectral profiles would suggest the *anti* rotamer to exhibit fluorescence emission, which cannot be explained by ESPIT).

4. Conclusions

The principal objective of the undertaken research project was to examine whether and how the rotational isomerism may affect benzophenone scaffolds substituted in the *ortho* position with minor organic pendants. In this respect, a bunch of selected *ortho* BP derivatives were systematically explored via both theoretical (quantum-chemical simulations) and experimental (spectroscopic measurements) methods of chemical cognition.

Duly noted, the findings arising from the performed investigation clearly demonstrate that the discussed phenomenon of rotamerism indeed applies to the foregoing class of compounds, leaving a tangible mark on their photo-related properties. In particular, such impact is most prominent for the *ortho*-BP molecules substituted with minor aprotic pendants, which can then concurrently take two stable conformations with respect to the central carbonyl fragment - *syn* and *anti*. Although the resultant isomers share the same topology of bonds, yet, they are unveiled to exhibit clearly distinct (photo)physical properties, manifested most of all in their diverse photoluminescence spectra. To wit, the emission profiles characterizing the foregoing *syn* and *anti* species, depending on the given *o*-BP entity, are observed to be shifted even up to 50 nm, which represents an indisputably substantial difference, rather rarely seen on such a scale for conformational systems. Additionally, the very nature of the spectra recorded for *ortho*-cyano- and *ortho*-methylbenzophenone strongly suggests that these compounds go through a fairly unique pathway of photorelaxation, that involves singlet rather than the anticipated triplet excited states. Being exceptional enough, this feature is believed to provide an interesting subject for future research aimed at its elucidation.

To conclude, the performed study allowed to shed some additional light onto certain intricacies behind the molecules comprising the widespread benzophenone scaffold. Although the presented findings belong solely to the domain of fundamental research, yet, better understanding of the subtleties that rule the foregoing compounds may in perspective translate also into their more conscious and thus efficient use in the application-oriented branches of chemistry.

Authors statements

Declaration of generative AI

The Authors declare that no generative artificial intelligence (AI) technologies have been employed in the writing process of this article.

CRediT authorship contribution statement

Andrzej J. Kałka: Writing – original draft, Software, Methodology, Investigation, Formal analysis, Conceptualization. **Aleksandra Orlef:** Methodology, Investigation. **Agnieszka Kaczor:** Writing – review & editing, Supervision, Resources. **Andrzej M. Turek:** Writing – review & editing, Supervision, Resources.

Declaration of competing interest

The authors declare that they have no known competing financial interests or personal relationships that could have appeared to influence the work reported in this paper.

Acknowledgments

The quantum-chemical calculations were performed thanks to the computational resources of the Ares and Eagle HPC clusters, provided respectively by the Academic Computer Centre Cyfronet AGH and Poznan Supercomputing and Networking Center (PSNC), both affiliated to the PLGrid Infrastructure consortium.

The Authors, led by AMT, wish to dedicate this paper to prof. Jack Saltiel from the Florida State University, Tallahassee, on the occasion of his more than sixty years of active research in the fields of photochemistry and photophysics, filled with outstanding scientific achievements and major milestones.

Supplementary materials

The online version of this article, found at doi:10.1016/j.molstruc.2025.143770, is additionally complemented with the electronic Supplementary Information (SI), comprising some auxiliary figures and tables that support findings presented within the original paper. The Reader is also provided with the set of digitalized spectroscopic data collected during the performed measurements (IR spectra and excitation-emission maps, EEM), depicting the original unscaled signal intensities.

Data availability

The data that supports the findings of this study are available within the article and its associated contents. Additional information is available from the Authors upon a reasonable request.

References

[1] Y.P. Sun, D.F. Sears, J. Saltiel, Resolution of benzophenone delayed fluorescence and phosphorescence spectra - evidence of vibrationally unrelaxed prompt benzophenone fluorescence, J. Am. Chem. Soc. 111 (1989) 706–711, https://doi.org/10.1021/ja00184a047.
[2] D.C. Sergentu, R. Maurice, R.W.A. Havenith, R. Broer, D. Roca-Sanjuán, Computational determination of the dominant triplet population mechanism in photoexcited benzophenone, Phys. Chem. Chem. Phys. 16 (2014) 25393–25403, https://doi.org/10.1039/c4cp03277b.
[3] G. Dormán, H. Nakannura, A. Pulsipher, G.D. Prestwich, The life of Pi Star: exploring the exciting and forbidden worlds of the benzophenone photophore, Chem. Rev. 116 (2016) 15284–15398, https://doi.org/10.1021/acs.chemrev.6b00342.
[4] K. Shizu, H. Kaji, Theoretical determination of rate constants from excited states: application to benzophenone, J. Phys Chem. A 125 (2021) 9000–9010, https://doi.org/10.1021/acs.jpca.1c06165.
[5] P.P. Levin, A.F. Efremkin, I.V. Khudyakov, Benzophenone as a photoprobe of polymer films, Chem. Phys. 495 (2017) 23–28, https://doi.org/10.1016/j.chemphys.2017.08.006.
[6] D. Blazevicius, S. Grigalevicius, A review of benzophenone-based derivatives for organic light-emitting diodes, Nanomaterials 14 (2024), https://doi.org/10.3390/nano14040356.
[7] K. Sivakumar, A. Nalini, Benzophenone type UVR filters for various materials: a review, J. Mol. Liq. 395 (2024) 123905, https://doi.org/10.1016/j.molliq.2023.123905.
[8] A.R. Heurung, S.I. Raju, E.M. Warshaw, Benzophenones, Dermatitis 25 (2014) 3–10, https://doi.org/10.1097/Der.0000000000000025.
[9] J.F. Mao, W.X. Li, C.N. Ong, Y.L. He, M.C. Jong, K.Y.H. Gin, Assessment of human exposure to benzophenone-type UV filters: a review, Environ. Int. 167 (2022) 107405, https://doi.org/10.1016/j.envint.2022.107405.
[10] S.B. Wu, C.L. Long, E.J. Kennell, Structural diversity and bioactivities of natural benzophenones, Nat. Prod. Rep. 31 (2014) 1158–1174, https://doi.org/10.1039/c4np00027g.
[11] K. Surana, B. Chaudhary, M. Diwaker, S. Sharma, Benzophenone: a ubiquitous scaffold in medicinal chemistry, Medchemcomm 9 (2018) 1803–1817, https://doi.org/10.1039/c8md00300a.
[12] A. Beckett, G. Porter, Primary photochemical processes in aromatic molecules. Part 10. -photochemistry of substituted benzophenones, Trans. Faraday Soc. 59 (1963) 2051–2057, https://doi.org/10.1039/tf9635902051.
[13] G. Porter, P. Suppan, Primary photochemical processes in aromatic molecules. Part 12. - excited states of benzophenone derivatives, Trans. Faraday Soc. 61 (1965) 1664–1673, https://doi.org/10.1039/tf9656101664.
[14] M.A. Garcia Garibay, W.S. Jenks, L. Pang, Heterogeneous hydrogen and deuterium transfer in the excited state of 2-methylbenzophenone in ether-pentane-alcohol glasses at 77 K, J. Photochem. Photobiol. A 96 (1996) 51–55, https://doi.org/10.1016/1010-6030(95)04300-4.

[15] B.M. Baughman, E. Stennett, R.E. Lipner, A.C. Rudawsky, S.J. Schmidtke, Structural and spectroscopic studies of the photophysical properties of benzophenone derivatives, J. Phys. Chem. A 113 (2009) 8011–8019, https://doi.org/10.1021/jp810256x.

[16] A.C. Bhasikuttan, A.K. Singh, D.K. Palit, A.V. Sapre, J.P. Mittal, Laser flash photolysis studies on the monohydroxy derivatives of benzophenone, J. Phys. Chem. A 102 (1998) 3470–3480, https://doi.org/10.1021/jp972375l.

[17] C.R. Groom, I.J. Bruno, M.P. Lightfoot, S.C. Ward, The Cambridge structural database, Acta Cryst. B 72 (2016) 171–179, https://doi.org/10.1107/S2052520616003954.

[18] P.J. Cox, D. Kechagias, O. Kelly, Conformations of substituted benzophenones, Acta Cryst. B 64 (2008) 206–216, https://doi.org/10.1107/S0108768108000232.

[19] F. Zuccarello, S. Millefiori, S. Trovato, Molecular-conformations of ortho-substituted benzophenones, Can. J. Chem. 54 (1976) 226–230, https://doi.org/10.1139/v76-035.

[20] A.A. Avdeenko, O.S. Pyshkin, V.V. Eremenko, M.A. Strzhemechny, L. M. Buravtseva, R.V. Romashkin, Photoluminescence of ortho-bromobenzophenone, Low Temp. Phys. 32 (2006) 1028–1034, https://doi.org/10.1063/1.2389009.

[21] M.A. Strzhemechny, S.G. Stepanian, D.I. Zloba, L.M. Buravtseva, O.S. Pyshkin, Y. P. Piryatinski, V.I. Melnik, G.V. Klishevich, L. Adamowicz, Scenario of temperature-related variation of phosphorescence spectra of ortho-bromobenzophenone crystal, Chem. Phys. 463 (2015) 58–64, https://doi.org/10.1016/j.chemphys.2015.10.002.

[22] G.P. Moss, Basic terminology of stereochemistry, Pure Apply Chem. 68 (1996) 2193–2222, https://doi.org/10.1351/pac199668122193.

[23] S.E. Blanco, J.J. Silber, F.H. Ferretti, Conformation, hydrogen bonding and UV solvatochromic shifts of benzophenones in primary alcohols, J. Mol. Struct. 582 (2002) 91–105, https://doi.org/10.1016/S0166-1280(01)00770-9.

[24] M. Hagiri, N. Ichinose, J. Kinugasa, T. Iwasa, T. Nakayama, Excited-state intramolecular proton transfer (ESIPT)-type phosphorescence of 2-aminobenzophenone in 77 K matrices, Chem. Lett. 33 (2004) 326–327, https://doi.org/10.1246/cl.2004.326.

[25] W. Li, J.D. Xue, S.C. Cheng, Y. Du, D.L. Phillips, Influence of the chloro substituent position on the triplet reactivity of benzophenone derivatives: a time-resolved resonance Raman and density functional theory study, J. Raman Spectrosc. 43 (2012) 774–780, https://doi.org/10.1002/jrs.3078.

[26] A.A. Lamola, L.J. Sharp, Environmental effects on the excited states of o-hydroxy aromatic carbonyl compounds, J. Phys. Chem. 70 (1966) 2634–2638, https://doi.org/10.1021/j100880a032.

[27] I. Baraldi, M.C. Bruni, M. Caselli, G. Ponterini, Rotamerism in 2,2′-binaphthyl - a study based on fluorescence analysis and Cs-indo/ci calculations, J. Chem. Soc. Farad. Trans. 2 (85) (1989) 65–74, https://doi.org/10.1039/f29898500065.

[28] B. Bhattacharya, B. Jana, D. Bose, N. Chattopadhyay, Multiple emissions of benzil at room temperature and 77 K and their assignments from quantum chemical calculations, J. Chem. Phys. 134 (2011) 044535, https://doi.org/10.1063/1.3533797.

[29] P. Kundu, S. Ghosh, N. Chattopadhyay, Exploration of photophysics of 2,2′-pyridil at room temperature and 77 K: a combined spectroscopic and quantum chemical approach, Photochem. Photobiol. Sci. 6 (2017) 159–169, https://doi.org/10.1039/c6pp00378h.

[30] R.A. Mata, M.A. Suhm, Benchmarking quantum chemical methods: are we heading in the right direction? Angew. Chem. Int. Edit. 56 (2017) 11011–11018, https://doi.org/10.1002/anie.201611308.

[31] A.J. Kałka, P. Ręka, J. Grolik, K. Ostrowska, A.M. Turek, Exploring rotational isomerism of fluorescent diarylethenes comprising 2-naphthyl and regioisomeric oxazoyl groups. A combined experimental and computational study, J. Mol. Struct. 1322 (2025), https://doi.org/10.1016/j.molstruc.2024.140611.

[32] Gaussian 16, Rev. A.03, Gaussian Inc., Wallingford (CT), 2016.

[33] A.D. Laurent, D. Jacquemin, TD-DFT benchmarks: a review, Int. J. Quantum Chem. 113 (2013) 2019–2039, https://doi.org/10.1002/qua.24438.

[34] V. Barone, M. Biczysko, J. Bloino, Fully anharmonic IR and Raman spectra of medium-size molecular systems: accuracy and interpretation, Phys. Chem. Chem. Phys. 16 (2014) 1759–1787, https://doi.org/10.1039/c3cp53413h.

[35] D. Jacquemin, I. Duchemin, X. Blase, 0-0 Energies using hybrid schemes: benchmarks of TD-DFT, CIS(D), ADC(2), CC2, and BSE formalisms for 80 real-life compounds, J. Chem. Theory Comput. 11 (2015) 5340–5359, https://doi.org/10.1021/acs.jctc.5b00619.

[36] M. Mendolicchio, J. Bloino, V. Barone, General perturb-then-diagonalize model for the vibrational frequencies and intensities of molecules belonging to Abelian and Non-Abelian symmetry groups, J. Chem. Theory Comput. 17 (2021) 4332–4358, https://doi.org/10.1021/acs.jctc.1c00240.

[37] M.W.D. Hanson-Heine, M.W. George, N.A. Besley, Calculating excited state properties using Kohn-Sham density functional theory, J. Chem. Phys. 138 (2013), https://doi.org/10.1063/1.4789813.

[38] J. Bloino, M. Biczysko, F. Santoro, V. Barone, General approach to compute vibrationally resolved one-photon electronic spectra, J. Chem. Theory Comput. 6 (2010) 1256–1274, https://doi.org/10.1021/ct9006772.

[39] A.M. Turek, G. Krishnamoorthy, K. Phipps, J. Saltiel, Resolution of benzophenone delayed fluorescence and phosphorescence with compensation for thermal broadening, J. Phys. Chem. A 106 (2002) 6044–6052, https://doi.org/10.1021/jp0200122.

[40] J.K. Kauppinen, D.J. Moffatt, H.H. Mantsch, D.G. Cameron, Fourier self-deconvolution - a method for resolving intrinsically overlapped bands, Appl. Spectrosc. 35 (1981) 271–276, https://doi.org/10.1366/0003702814732634.

[41] P.B. Tooke, Fourier self-deconvolution in IR spectroscopy, Trends Anal. Chem. 7 (1988) 130–136, https://doi.org/10.1016/0165-9936(88)87010-9.

[42] M.F. Wahab, F. Gritti, T.C. O'Haver, Discrete fourier transform techniques for noise reduction and digital enhancement of analytical signals, Trends Anal. Chem. 143 (2021), https://doi.org/10.1016/j.trac.2021.116354.

[43] A.J. Kalka, A.M. Turek, Searching for alternatives to the Savitzky-Golay filter in the spectral processing domain" (vol 77, Pg 426, 2023), Appl. Spectrosc. 77 (2023), https://doi.org/10.1177/00037028231181097, 1095-1095.

[44] A. de Juan, J. Jaumot, R.A. Tauler, Multivariate curve resolution (MCR). Solving the mixture analysis problem, Anal. Methods 6 (2014) 4964–4976, https://doi.org/10.1039/c4ay00571f.

[45] A.J. Kałka, A.M. Turek, Do spectra live in the matrix? A brief tutorial on applications of factor analysis to resolving spectral datasets of mixtures, J. Fluoresc. 31 (2021) 1599–1616, https://doi.org/10.1007/s10895-021-02753-w.

[46] E.R. Henry, The use of matrix methods in the modeling of spectroscopic data sets, Biophys. J. 72 (1997) 652–673, https://doi.org/10.1016/S0006-3495(97)78703-4.

[47] S. Wold, K. Esbensen, P. Geladi, Principal component analysis, Chemom. Intell. Lab. Syst. 2 (1987) 37–52, https://doi.org/10.1016/0169-7439(87)80084-9.

[48] W.H. Lawton, E.A. Sylvestre, Self modeling curve resolution, Technometrics 13 (1971) 617–633, https://doi.org/10.2307/1267173.

[49] K. Sasaki, S. Kawata, S. Minami, Estimation of component spectral curves from unknown mixture *appl*, Optics 23 (1984) 1955–1959, https://doi.org/10.1364/Ao.23.001955.

[50] A. Meister, Estimation of component spectra by the principal components method, Anal. Chim. Acta 161 (1984) 149–161, https://doi.org/10.1016/S0003-2670(00)85786-4.

[51] R. Rajkó, K. István, Analytical solution for determining feasible regions of self-modeling curve resolution (SMCR) method based on computational geometry, J. Chemom. 19 (2005) 448–463, https://doi.org/10.1002/cem.947.

[52] P.H.C. Eilers, B.D. Marx, Flexible smoothing with B-splines and penalties, Stat. Sci. 11 (1996) 89–102, https://doi.org/10.1214/ss/1038425655.

[53] W.F. Maddams, The scope and limitations of curve fitting, Appl. Spectrosc. 34 (1980) 245–267, https://doi.org/10.1366/0003702804730312.

[54] J.H.Z. Huang, H.P. Shen, A. Buja, The analysis of two-way functional data using two-way regularized singular value decompositions, J. Am. Stat. Assoc. 104 (2009) 1609–1620, https://doi.org/10.1198/jasa.2009.tm08024.

[55] M.C. Yappert, J.D. Ingle, Correction of polychromatic luminescence signals for inner-filter effects, Appl. Spectrosc. 43 (1989) 759–767, https://doi.org/10.1366/0003702894202120.

[56] M. Kubista, R. Sjoback, S. Eriksson, B. Albinsson, Experimental correction for the inner-filter effect in fluorescence-spectra, Analyst 119 (1994) 417–419, https://doi.org/10.1039/an9941900417.

[57] MATLAB, v.R2015a, The MathWorks Inc, Natic (MA), 2015.

[58] Anon, Origin Pro 9.1, OriginLab Corporation, Northampton, 2014.

[59] M. Kasha, Characterization of electronic transitions in complex molecules, Discuss. Faraday Soc. 9 (1950) 14–19, https://doi.org/10.1039/df9500900014.

[60] J.C. del Valle, J. Catalán, Kasha's rule: a reappraisal, Phys. Chem. Chem. Phys. 21 (2019) 10061–10069, https://doi.org/10.1039/c9cp00739c.

[61] H.J.C. Jacobs, E. Havinga (1979). Photochemistry of vitamin D and its isomers and of simple trienes. In Advances in: Photochemistry pp. 305-373, DOI: 10.1002/9780470133415.ch4.

[62] J.K. Whitesell, M.A. Minton, V.D. Tran, The non-equilibration of excited rotamers (NEER) principle. Ground-state conformational bias in triene photocyclizations, J. Am. Chem. Soc. 111 (1989) 1473–1476, https://doi.org/10.1021/ja00186a049.

[63] J.B. Birks, D.J. Dyson, B.H. Flowers, The relations between the fluorescence and absorption properties of organic molecules, Proc. R. Soc. A 275 (1963) 135–148, https://doi.org/10.1098/rspa.1963.0159.

[64] I.B. Berlman, On an empirical correlation between nuclear conformation and certain fluorescence and absorption characteristics of aromatic compounds, J. Phys. Chem. 74 (1970) 3085–3093, https://doi.org/10.1021/j100710a012.

[65] Z. Pawelka, A. Koll, T. Zeegers-Huyskens, Solvent effect on the conformation of Benzil, J. Mol. Struct. 597 (2001) 57–66, https://doi.org/10.1016/S0022-2860(01)00593-2.

[66] N. Marcotte, S. Fery-Forgues, Spectrophotometric evidence for the existence of rotamers in solutions of some ketocyanine dyes, J. Photochem. Photobiol. A 130 (2000) 133–138, https://doi.org/10.1016/S1010-6030(99)00213-0.

[67] T.M. Kolev, B.A. Stamboliyska, Vibrational spectra and structure of benzophenone and its 18O and d10 labelled derivatives: an ab initio and experimental study, Spectrochim. Acta A 56 (2000) 119–126, https://doi.org/10.1016/S1386-1425(99)00123-7.

[68] A. Beckett, G. Porter, Primary photochemical processes in aromatic molecules. Part 9.—Photochemistry of benzophenone in solution, Trans. Faraday Soc. 59 (1963) 2038–2050, https://doi.org/10.1039/TF9635902038.

[69] J.R. Lakowicz, Quenching of Fluorescence in: Principles of Fluorescence Spectroscopy, Springer US, Boston (MA), 1983, pp. 257–301, https://doi.org/10.1007/978-1-4615-7658-7_9.

[70] G.H. Huang, C. Zhou, R.H. Liang, S.S. Sun, Z.Q. Deng, J.Y. Li, L. Dang, D.L. Phillips, M.D. Li, Ultrafast time-resolved spectroscopic study on the photophysical and photochemical reaction mechanisms of methylbenzophenone in selected solutions, J. Phys. Chem. B 126 (2022) 9388–9398, https://doi.org/10.1021/acs.jpcb.2c06452.

[71] M. Mukai, S. Yamauchi, N. Hirota, J. Higuchi, Time-resolved epr and phosphorescence studies of the lowest excited triplet-state of benzil, J. Phys. Chem. 96 (1992) 9328–9331, https://doi.org/10.1021/j100202a050.

[72] A. Sarkar, S. Chakravorti, Photo-rotamerism of 2,2′-pyridil in different environments: a quest for geometry in excited states, J. Luminesc. 69 (1996) 161–168, https://doi.org/10.1016/0022-2313(96)00091-9.
[73] M.W. Wolf, R.E. Brown, L.A. Singer, Deactivation of benzophenone triplets via exciplex formation - evidence for dual reaction pathways, J. Am. Chem. Soc. 99 (1977) 526–531, https://doi.org/10.1021/ja00444a036.
[74] N.J. Turro, M. Aikawa, I.R. Gould, The laser vs the lamp - a novel laser-induced adiabatic reaction and luminescence of benzophenone, J. Am. Chem. Soc. 104 (1982) 856–858, https://doi.org/10.1021/ja00367a040.
[75] J.B. Birks, Excimers, Rep. Prog. Phys. 38 (1975) 903–974, https://doi.org/10.1088/0034-4885/38/8/001.